Environmental Science & Technology

ARTICLE

pubs.acs.org/est

Measurements of Aerosol Chemistry during New Particle Formation Events at a Remote Rural Mountain Site

Jessie M. Creamean,[†] Andrew P. Ault,[†,⊥] John E. Ten Hoeve,[‡] Mark Z. Jacobson,[‡] Gregory C. Roberts,[§,∥] and Kimberly A. Prather[†,§,*]

[†]Department of Chemistry and Biochemistry, University of California, San Diego, La Jolla, California 92093-0314, United States

[‡]Department of Civil & Environmental Engineering, Stanford University, Stanford, California 94305, United States

[§]Scripps Institution of Oceanography, University of California, San Diego, La Jolla, California 92093, United States

[∥]Centre National de Recherches Météorologiques—Groupe d'étude de l'Atmosphère Météorologique (GAME), Toulouse, France

Supporting Information

ABSTRACT: Determining the major sources of particles that act as cloud condensation nuclei (CCN) represents a critical step in the development of a more fundamental understanding of aerosol impacts on cloud formation and climate. Reported herein are direct measurements of the CCN activity of newly formed ambient particles, measured at a remote rural site in the Sierra Nevada Mountains of Northern California. Nucleation events in the winter of 2009 occurred during two pristine periods following precipitation, with higher gas-phase SO_2 concentrations during the second period, when faster particle growth occurred (7−8 nm/h). Amines, as opposed to ammonia, and sulfate were detected in the particle phase throughout new particle formation (NPF) events, increasing in number as the particles grew to larger sizes. Interestingly, long-range transport of SO_2 from Asia appeared to potentially play a role in NPF during faster particle growth. Understanding the propensity of newly formed particles to act as CCN is critical for predicting the effects of NPF on orographic cloud formation during winter storms along the Sierra Nevada Mountain range. The potential impact of newly formed particles in remote regions needs to be compared with that of transported urban aerosols when evaluating the impact of aerosols on clouds and climate.

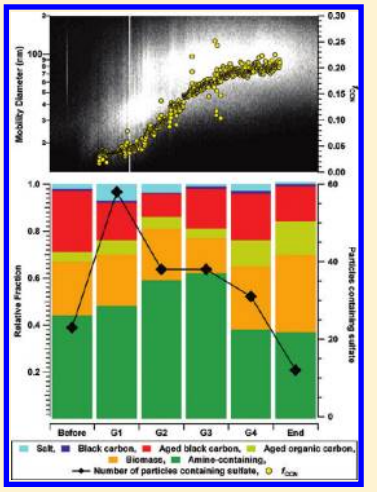

1. INTRODUCTION

Aerosols are ubiquitous in the troposphere and profoundly impact climate.[1] They scatter and absorb incoming short wave and outgoing long wave radiation, and act as cloud condensation nuclei (CCN) affecting cloud radiative and physical properties. Under supersaturated conditions, CCN compete for available water vapor, creating large populations of small-sized cloud droplets increasing the reflectivity of clouds.[2,3] Smaller, more numerous cloud droplets often cannot grow to large enough sizes to precipitate.[2]

The impact of aerosols on clouds, referred to as the indirect effect, represents arguably the largest single source of uncertainty out of all contributors to global radiative forcing estimates,[1] and therefore a better understanding of the sources of the aerosols that determine the magnitude of this effect is needed. In situ formation of ultrafine particles (≤100 nm) through gas-to-particle conversion of low volatility vapors represents a significant source of tropospheric aerosols, especially in remote environments. The initial critical clusters must grow into larger sizes to activate as CCN, and thus become relevant for cloud formation.[4] Determining the magnitude and mechanistic drivers of the nucleation and growth processes of newly formed particles that ultimately become effective CCN will improve regional and global climate models.[5]

New particle formation (NPF) involves two important steps.[6] The first step involves homogeneous or ion-induced nucleation of neutral or ion clusters and the second step involves the growth of these clusters into larger particles.[7−9] In most cases, pristine ambient conditions with lower relative humidity represent favorable conditions for particle nucleation,[10] whereas higher relative humidities[11] and lower temperatures[9] provide favorable conditions for the subsequent growth of newly formed particles, depending on the species involved. Formation of new particles is affected by the production of condensable vapor precursors, such as H_2SO_4, formed from oxidation of SO_2.[12] Originally, it was hypothesized that the initial step involved cluster formation by H_2SO_4 and water vapor and that H_2SO_4 was also responsible for the subsequent growth of the clusters, however, the involvement of H_2SO_4 alone cannot explain the formation and growth rates of

Received: November 1, 2010
Accepted: August 2, 2011
Revised: June 21, 2011

dx.doi.org/10.1021/es103692f | Environ. Sci. Technol. XXXX, XXX, 000–000

observed particle formation.[13] Therefore, other species in addition to H_2SO_4 must contribute to the growth of new particles via condensation and/or heterogeneous reactions.[14] Species that have sufficiently low volatility so as to be involved with nucleation are also capable of participating in the subsequent growth, and as particle size increases, so too do the number of possible condensable species and mechanisms. More is known about the species that contribute to particle growth, such as NH_3[15] or as shown more recently semivolatile organic species[5,11] than about the species involved with the nucleation process. More specifically, formation of aminium salts has been modeled[16] and these species have been detected in newly formed particles.[17,18] Amines form salts with organic and inorganic acids during particle growth,[14,19] supporting the hypothesis that amines/nitrogen-containing organics and H_2SO_4 play a role in the growth of new particles.

Because of instrumental challenges involved in measuring the chemistry of 1−3 nm particles, the molecular identities of the species involved have eluded scientists for many years. As a result, chemical composition is typically inferred for newly formed particles by utilizing multiple measurements. Mäkelä et al. (2001) detected dimethylammonium ($(CH_3)_2NH_4^+$) using 2-stage cascade impactors and ion chromatography during NPF events.[17] Although they were able to identify species down to 5 nm, the time resolution was low and aminium sulfate ($(HNR_3)_2SO_4$) was inferred from the correlation of bulk particle measurements of $(CH_3)NH_2^+$ and sulfate. Smith et al. (2004) measured nitrogen-containing organics and sulfate using a Thermal Desorption Chemical Ionization Mass Spectrometer (TDCIMS). They detected particles from 10 to 30 nm with 5−10 min time resolution and found that nitrogen-containing organics played a significant role in the growth of nanoparticles.[20] Chemical measurements at these small sizes represent a significant advancement in the characterization of newly formed particles. However, the TDCIMS cannot measure amines and sulfate simultaneously in the same particle and therefore questions remain about the associations between amines and sulfate at the single particle level during NPF events.

The challenge with using bulk measurements to determine the primary species involved in particle formation is that the measured mass concentrations represent the average chemical composition of many particles. For instance, when amines and sulfate are detected in particles collected on filters, the detected species can actually occur in separate particles. Single-particle mixing state measurements show whether two species are present within a single particle, a level of detail that is critical for understanding the key species involved in particle formation and growth processes. In the current work, aerosol time-of-flight mass spectrometry (ATOFMS) was used to provide dual polarity, single-particle analysis during NPF events in real-time at a remote rural region in the Sierra Nevada Mountains in Northern California. We report the first observations of nitrogen-containing organic species and sulfate within the same particles after significant particle growth during NPF events. Understanding the sources of the species involved in new particle formation is critical as this could be an important local source of CCN in the Sierra Nevada. Previous studies have suggested that CCN were transported directly from California's Central Valley (CV),[21] however, in situ NPF between amines from the CV and long-range transported SO_2 from Asia could also contribute as a CCN source in the Sierra Nevada as described herein.

2. EXPERIMENTAL SECTION

Ground-based aerosol measurements were made during the CalWater Early Start field campaign during the late winter at the Sugar Pine Reservoir in Foresthill, CA, a remote rural site in the Sierra Nevada Mountains (39° 07′ 42.80″ N, 120° 48′ 04.90″ W; elevation ∼1064 m ASL). Particle size distributions were measured between 11 and 604 nm using a scanning mobility particle sizer (SMPS) (Model 3936 L, TSI Inc.). Meteorological measurements including temperature, relative humidity, wind direction, solar radiation, and precipitation were acquired from colocated instruments operated by the National Oceanic and Atmospheric Administration (NOAA). Gas-phase O_3 and SO_2 concentrations were measured using an O_3 analyzer (Model 49C, Thermo Environmental Instruments, Inc.) and a SO_2 analyzer (43C, Thermo Environmental Instruments, Inc.), respectively. Due to calibration problems with the SO_2 analyzer, SO_2 is presented as relative concentrations. Black carbon mass concentrations were measured using a seven wavelength aethalometer (Model AE31, Magee Scientific). CCN concentrations were measured at 0.3% supersaturation using a compact streamwise thermal-gradient diffusion chamber.[22] Only periods with reliable CCN data are presented. A condensation particle counter (CPC) (Model 3010, TSI Inc.) was used to determine condensation nuclei (CN) concentrations, which were compared to the number concentration of $CCN_{0.3}$ to determine the activated fractions.

An ultrafine (UF)-ATOFMS, a modified version of the standard ATOFMS,[23] was utilized for individual aerosol aerodynamic sizing and chemical composition. The UF system is described in detail in Su et al. (2004).[24] The UF-ATOFMS measures the vacuum aerodynamic size ($100 \leq D_{va} \leq 1000$ nm) and chemical composition of particles by laser desorption/ionization which allows us to obtain dual polarity mass spectra.[23,24] D_{va} is related to the electric mobility diameter (D_{me}) measured by the SMPS through effective density and is discussed in detail elsewhere.[25] During the study, 1 146 366 particles were chemically analyzed from 2/21/09 to 3/10/09 (PST). Single-particle mass spectra were imported into YAADA (www.yaada.org), a software toolkit in Matlab (The Mathworks, Inc.), for detailed analysis of particle size and chemistry. ART-2a, an adaptive resonance theory-based clustering algorithm,[26] was then used to group single-particle mass spectra with a vigilance factor of 0.80. ART-2a classifies particles into separate clusters depending on the presence and intensity of ion peaks in the respective mass spectra. The most populated 70 clusters account for > 90% of the total ART-2a classified particles. Peak identifications in this work correspond to the most probable ions for a given m/z ratio based on previous lab and field studies.

3. RESULTS AND DISCUSSION

3.1. Ambient Conditions for NPF. Figure 1a shows SMPS, temperature, and relative humidity (RH) data obtained during the study. One polluted period impacted by transport from the CV occurred from 2/21−2/23. NPF events occurred during cleaner periods following precipitation between the dates of 2/24−2/28 (denoted as P1) and 3/6−3/8 (denoted as P2) as shown by high number concentrations in white. Particularly, NPF events had high number concentrations starting at small sizes (∼11−15 nm) followed by subsequent growth to larger

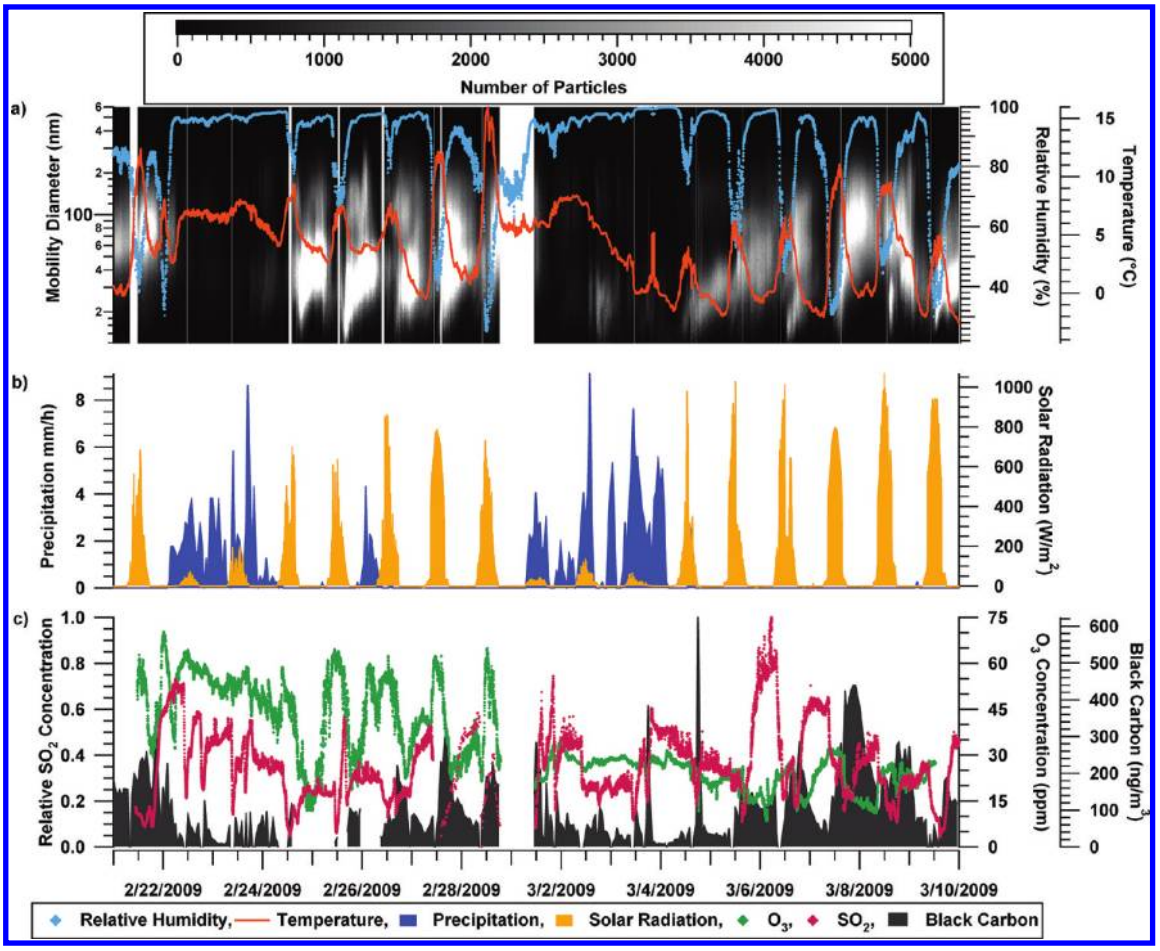

Figure 1. (a) 5-min temporally resolved SMPS size distributions (nm) with superimposed 2-min relative humidity (%) and temperature (°C), (b) hourly precipitation (mm/h) and 2-min solar radiation (W/m^2), and (c) hourly gas-phase relative SO_2 and O_3 (ppm) concentrations and black carbon concentrations (ng/m^3).

sizes (~70−100 nm). All NPF events started in the late afternoon between ~14:00−16:00 during low RH, high temperature, and increased solar radiation, followed by particle growth as RH increased and temperature and solar radiation decreased. Mäkelä et al. (2001) previously observed NPF events during the afternoons in boreal forest locations.[17] Particle nucleation occurs when there is a reduction in total particle surface area, which often occurs immediately following precipitation events.[27] Precipitation removes the atmospheric "seed" particles that low volatility gases would normally condense upon. When elevated gas-phase concentrations are produced by increased solar radiation after precipitation, these species undergo oxidation processes and then homogeneously nucleate to form new particles. This series of events is shown in Figure 1a,b, when both NPF periods occurred after periods of precipitation. Clean conditions at the start of the NPF periods are typified by overall low mass concentrations (<185 ng/m^3) of black carbon (BC). BC or soot, formed from combustion sources, serves as an excellent tracer for the presence anthropogenic aerosols.[28] Figure 1c shows BC concentrations over the course of the study, which were low (average ± standard deviation =142.2 ± 97.8 ng/m^3 during NPF periods) compared to urban environments (on the order of 1−5 $\mu g/m^3$).[29] The Supporting Information contains an additional discussion of BC concentrations.

The precipitation periods showed fairly steady decreases in O_3 (ppm) and relative SO_2 concentrations (Figure 1c). O_3 concentrations were higher during P1 compared to P2, whereas SO_2 concentrations were higher during P2 compared to P1. This suggests that different chemical processes and species were involved during the two NPF periods, as discussed below. During P1, SO_2 varied diurnally, first increasing from ~11:00 the previous day to ~1:00 the day of the NPF events while during P2, SO_2 started increasing at ~20:00 the days previous to both of the NPF events. However, O_3 was consistent during both NPF periods, peaking ~10:00−13:00 on the day of the events. Interestingly, the O_3 maxima occurred 2−5 h before the NPF events, and then decreased to a minimum, 4−9 h after the start of the NPF events. Lunden et al. (2006) observed a similar trend with O_3 peaking ~4 h before NPF at Blodgett Forest Research Station, a site with similar conditions ~16 miles southeast of Sugar Pine.[9] In the current work, SO_2 decreased from higher, steady concentrations as O_3 and solar radiation increased and before new particles started to form. Observed trends of SO_2 and O_3 in relation to NPF events suggest their involvement in new particle formation and growth processes, as suggested by Berndt et al. (2010) who previously observed NPF from reaction of OH (formed from O_3) and SO_2 in a laboratory setting.[30]

3.2. Growth of New Particles into CCN. Heavy precipitation periods resulting in clean conditions in conjunction with the

dx.doi.org/10.1021/es103692f |*Environ. Sci. Technol.* XXXX, XXX, 000–000

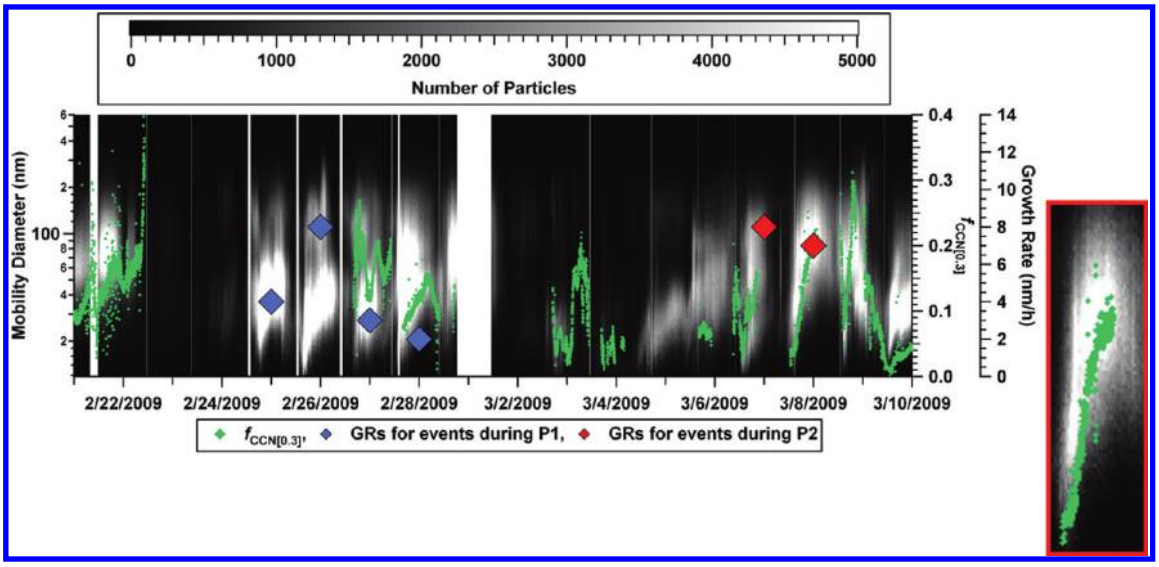

Figure 2. SMPS plotted with $f_{CCN[0.3]}$. The inset is the strongest correlation of $f_{CCN[0.3]}$ with an NPF event (3/7−3/8). The markers superimposed over each NPF event are the estimated GRs for the event on that day. Blue and red markers represent GRs during P1 and P2, respectively.

presence of necessary gas-phase species that induced NPF produced periods typified by the fast growth of newly formed particles. Frequent observations of the nucleation of particles only a few nanometers in diameter followed by subsequent growth to ∼100 nm have been shown to occur within 1−2 days in the continental boundary layer.[31] However, during the current work, we calculated the upper limit of growth to 100 nm to occur in as rapidly as 15 h. Having a measure of the time it takes a particle to grow up to 100 nm provides a relevant link between newly formed particles and those particles that can activate as CCN. Inferred growth rates (GRs) in Figure 2 and Table S1 of the were determined using the method discussed by Kulmala et al. (2004)[31] and are described in the Supporting Information. Briefly, lines were fit to the increasing mean particle sizes during NPF events. The GRs were calculated from the slopes of these fitted lines. According to Kulmala et al. (2004), uncertainties such as distinguishing between new and pre-existing particles and the exact start and end times of these events can lead to uncertainties in the GRs,[31] however, the times and sizes were chosen to limit contributions from these uncertainties as much as possible.

As shown in Figure 2, new particles grew faster on average during P2 compared to P1: inferred GRs during P1 and P2 were 4 ± 3 nm/h and 7 ± 1 nm/h, respectively. The difference in inferred GRs between P1 and P2 was most likely due to the involvement of different species as suggested by the air mass trajectories and different concentrations of key gas-phase species, namely O_3 and SO_2, during the two periods. In addition, higher concentrations of organic species due to higher average temperatures[32] could have contributed to the faster growth rates, on average, observed during P2 (as discussed in the Supporting Information). Because amines are basic compounds, they have the potential to undergo rapid acid−base reactions to form salts in/on particles in the presence of sulfuric acid, depending on temperature, the identity of the amine, and the concentrations and identities of acidic species present.[19] Higher SO_2 concentrations during P2 potentially led to more sulfuric acid in the newly formed particles making them more acidic, which can induce faster growth through acid−base reactions. Overall, inferred GRs from both periods (2−8 nm/h), particularly during P2, occur on the higher end of previously reported GR ranges for remote rural areas presented by Kulmala et al. (2004) and references therein.[31] Notably, GRs during the closely located Blodgett study (1−7 nm/h) were comparable to these measurements at Sugar Pine.[9]

One of the primary goals of the CalWater field campaign involved developing a better understanding of the sources of CCN that ultimately impact orographic clouds and precipitation in the Sierra Nevada. It has been hypothesized that the majority of CCN are transported from the polluted CV near Fresno and Bakersfield, a region with high agricultural activity.[21] However, it is possible that local NPF events such as the ones described here can produce large numbers of ultrafine particles that can ultimately grow and become CCN, especially in regions with a low anthropogenic influence at higher elevations.[33] Figure 2 shows the size distribution from Figure 1a along with the ratio of $CCN_{0.3}$ to all CN ($f_{CCN[0.3]}$). Importantly, increases in $f_{CCN[0.3]}$ coinciding with the NPF events during particle growth suggest these newly formed particles can effectively serve as CCN. These findings are consistent with recent studies which have also suggested that newly formed particles evolve into CCN through modeling[34−36] and observations in remote regions with similar conditions during NPF.[37,38]

3.3. Single-Particle Chemical Composition during NPF Events. To better understand the chemistry of the newly formed CCN, a more detailed look at particles in the typical CCN size range is merited. Data showing real-time changes in the chemical composition of larger, detectable sizes (>100 nm) have recently been used to provide insight into the chemistry of newly formed particles.[39] Since the UF-ATOFMS measures particles with $D_{va} \geq 100$ nm, we can only state that the detected species were likely involved in the initial formation and/or growth processes, which is why this term "NPF" is used throughout the work. However, it is likely that the chemical composition of particles from $100 \leq D_{va} \leq 1000$ nm is a product of condensation, heterogeneous reactions, and coagulation processes occurring during NPF events. To look at the chemistry in detail, P1 was further divided into shorter time periods based on the SMPS

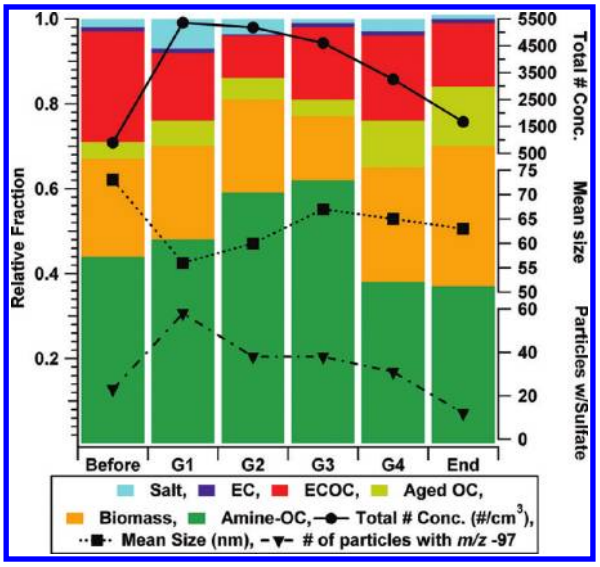

Figure 3. ATOFMS particle types in the 100−1000 nm size range measured during P1. Also pictured are the SMPS total particle number concentrations (#/cm^3), SMPS mean sizes (nm), and number of ATOFMS sulfate-containing (m/z −97) particles during each subperiod. All of these values are averaged over the four NPF events in P1.

data, including before events (non-NPF), growth subperiods G1 (≤20 nm), G2 (20−25 nm), G3 (25−30 nm), G4 (≥30 nm at higher number concentrations), and end of events (≥30 nm at lower number concentrations). Limited chemical data were obtained during P2 due to instrumental issues; therefore, this period was excluded when looking at chemistry during subperiods. However, a comparison of chemical species between P1 and species from the limited data collected during P2 is provided in the Supporting Information. The initial growth, or the G1 and G2 subperiods, typically corresponded to the smallest mean sizes and highest number concentrations compared to before and after the events, which is typical of NPF bursts.[40] Figure 3 shows the overall particle chemistry from 100 ≤ D_{va} ≤ 1000 nm from before the events, growth subperiods, and the end of events, along with the average number concentrations and mean sizes from the SMPS data. The major types observed at Sugar Pine included amine-containing organic carbon (amine-OC), aged organic carbon (aged OC), elemental carbon (EC), EC mixed with OC (ECOC), biomass, salts, and other minor particle types that consisted of < 1% of the total number of particles present during NPF. EC, ECOC, biomass, and salts were transported from other regions and clearly not formed during NPF events. Mass spectra and details of these other particle types are included in the Supporting Information.

As shown in Figure 3, the largest number fractions during NPF belonged to the amine-OC, biomass, and ECOC particle types, which represented 50%, 22%, and 16% of the total particle counts, respectively. Amine-OC types were characterized by markers at m/z 86 ($(C_2H_5)_2NCH_2^+$), 101 ($(C_2H_5)_3N^+$), 102 ($(C_2H_5)_3NH^+$), 118 ($(C_2H_5)_3NOH^+$), and other carbonaceous ions.[41,42] Not only was the amine-OC type the largest fraction, it increased as the newly formed particles grew into larger sizes, then decreased toward the end of the events. Before the events, amine-OC types comprised on average 44% of the total particle counts then increased to 48% during G1, 59% during G2, 62% during G3, then decreased to 38% during G4 and 37% during the end of events. Amine-OC particles also increased at the smallest sizes observable by the UF-ATOFMS (D_{va} = 100−300 nm) during the initial growth subperiods as shown/discussed in the Supporting Information. This trend suggests the presence of background amine-containing particles; the large increase in small-sized amine-OC particles during the initial growth subperiods suggests semivolatile amine species played a role in the growth of new particles. The amine-OC fraction did not increase as much as one might expect during G1 because the UF-ATOFMS sees larger sizes (D_{va} ≥ 100 nm) and thus does not directly measure the chemistry of the smallest particles during the initial growth periods of NPF. The decrease toward the end of events when particle number concentrations decreased suggests the amine-OC particles coagulated with other types of particles. Increases of amine species were observed from the beginning to the end of NPF events on aged OC, biomass, and ECOC particle types. By using digital color histograms of single particles we were able to monitor the evolution of the UF-ATOFMS particles types, which showed increases in the overall number of particles with amine species (m/z 86), and showed the major particle types, aged OC, biomass, and ECOC, coagulated with the small, newly formed amine-containing particles (see Supporting Information).

The increase in average number fraction as well as the absolute amine peak areas (Supporting Information) suggests amine species were involved in the growth of new particles. As previously mentioned, sulfate is also believed to play a role in NPF. Figure 3 shows the number of particles within all particle types containing the sulfate ion marker (m/z −97, HSO_4^-) per 5-min interval. The average number of particles containing m/z −97 followed a similar trend to the SMPS number concentration: lower numbers before events followed by higher numbers during initial growth subperiods, ending with lower numbers toward the end.

Both the number of particles containing sulfate and the number and overall fraction of amine-OC particles increased during the initial growth subperiods compared to before the events and decreased at the end of the events, suggesting that these species played a role in the growth of new particles. Figure 4a shows the SMPS data with the fraction of amine-OC particles containing sulfate and total number of particles per 15-min interval. Panel (a) in Figure S3 of the Supporting Information corresponds to the mass spectra for amine-OC particles containing sulfate. Increases in the fraction of amine-OC particles containing sulfate were observed during NPF events, providing clear evidence that amines and sulfate were indeed present in the same, single particles. In addition, the fractions of amine-OC particles containing sulfate were highest mainly during the beginning on NPF events, likely due to the large number concentrations of aminium sulfate particles formed during the NPF bursts. The ability to measure both amine and sulfate species in the same single particles during NPF directly confirms these aminium salts formed, supporting previous inferences of their existence in newly formed particles.

Figure 4b shows a correlation plot of the fraction of particles with m/z 86 versus the fraction with m/z −97 as a function of study date (in color), with the black line representing the 1:1 line. The color matches the respective date and time of markers in Figure 4a. Each marker represents the fraction of particles containing m/z 86 and/or m/z −97 in 15-min intervals. Three notable groups of points exist with similar colors on the 1:1 line, meaning those points contain roughly equivalent numbers of particles with m/z 86 and m/z −97. The orange group of points (upper right) represents the period of high particle number

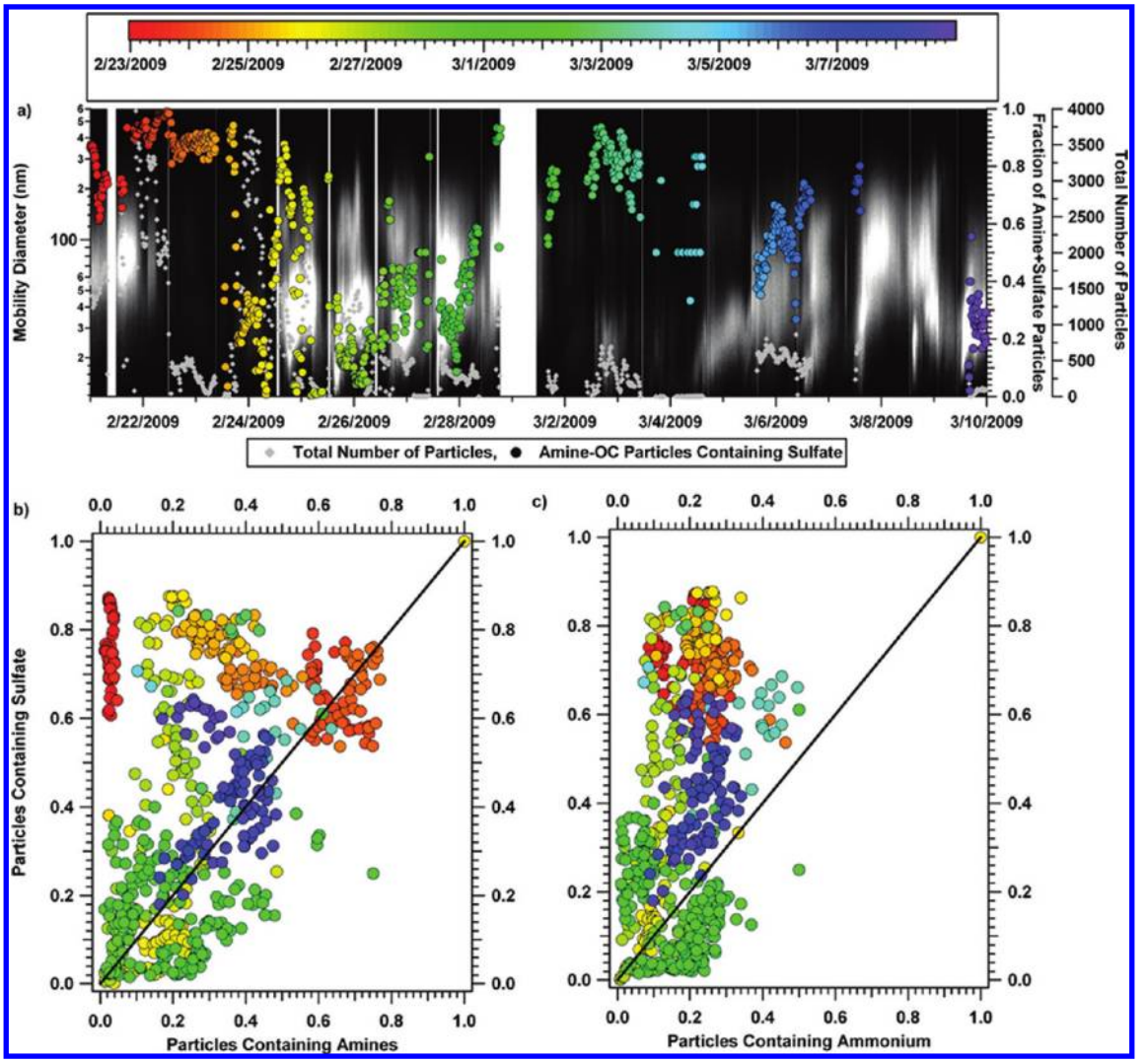

Figure 4. (a) SMPS plotted with the fraction of amine-OC particles containing sulfate (out of the total number of particles) as a function of study date and time in color and the total number of particles. (b) Correlation of the fraction of particles with sulfate (m/z −97) to fraction of particles with amines (m/z 86) also as a function of study date and time. The black line represents the 1:1 line. (c) Similar correlation plot to (b), but with ammonium (m/z 18) in place of m/z 86. Each marker in all panels represents the fraction of particles per 15-min interval.

concentrations, but was not an NPF event. The yellow/green group of points falls within the first NPF period from 2/24−2/28, whereas the blue group of points falls within the second NPF period from 3/6−3/8. Figure 4c shows a similar plot with ammonium ($^{18}NH_4^+$) in place of m/z 86, since ammonium has been shown to contribute to particle nucleation.[8,43] However, a 1:1 correlation was not observed between ammonium (m/z 18) and sulfate, suggesting ammonium played a different role in nucleation and particle growth. It is possible that ammonium was involved with the initial cluster formation. Previous studies have expressed the significance of aminium salt formation in ambient aerosol[42] and ammonium displacement with aminium species in secondary organic aerosol[19] and after the initial formation process during NPF in a laboratory setting.[44] On the basis of this combination of new results and previous studies, it appears that H_2SO_4 was involved with formation with additional growth from amines at larger particle sizes, forming predominantly aminium-sulfate salts.

3.4. Potential Sources of Gas-Phase Species Involved in New Particle Growth. Although ambient conditions were similar between P1 and P2 (temperature, RH, solar radiation, and pristine air), higher O_3 concentrations were observed during P1 compared to P2 but in contrast, higher SO_2 concentrations occurred during P2 compared to P1. Differences between the two periods can be explained by different air masses impacting the site that transported the species involved in NPF.

Regional airflows were investigated with back trajectories simulated by the Lagrangian model FLEXPART[45,46] to provide insight into the source regions of species potentially playing a role in NPF. O_3 and SO_2 exhibited diurnal behavior during both NPF periods, due to upslope and downslope airflows that are common in this region; the daytime upslope flow (strongest ∼12:00−13:00) transports species from the CV, while the nighttime downslope flow (strongest ∼2:00−3:00) carries pollutants toward the Valley floor.[47,48] This diurnal behavior also occurred in O_3 measurements at Blodgett and was attributed to the upslope/downslope system, suggesting O_3 came from the CV.[9] In the current work, O_3 concentrations peaked ∼10:00−13:00, which coincided with the strongest upslope flow times. In the CV, O_3 forms in photochemical urban pollution,[43] common in cities

dx.doi.org/10.1021/es103692f |Environ. Sci. Technol. XXXX, XXX, 000–000

including Sacramento and Fresno. In contrast, during P2 SO_2 peaked during the downslope flow, suggesting it was not transported from the CV.

During P2, long-range transport of SO_2 at higher altitudes, which could potentially become entrained from the free troposphere during the day and descend into the stable nighttime boundary layer,[49] appears to be the difference between the two periods and led to higher SO_2 at the site during P2. NASA's Ozone Monitoring Instrument (OMI) sensor onboard the Aura satellite measures backscattered radiation which is used to estimate vertically integrated SO_2 values. Images acquired for the days before, during, and after NPF events for both periods are shown in the Supporting Information. Background levels of SO_2 were observed in Northern California on 2/26. On the same day, an SO_2 plume from the coast of Asia traveled across the Pacific Ocean from 2/26−3/5, arriving off the coast of Washington and ultimately Northern California between 3/6−3/8, corresponding to the peak in SO_2 concentrations. Levels of SO_2 returned to background levels on 3/9, similar to those measured on 2/26. Back trajectories (also shown in the Supporting Information) further support trans-Pacific transport during P2, following a high pressure system that provided clear skies and dry conditions known to inhibit in-cloud conversion of SO_2 to sulfate. Together, OMI data and back trajectory analysis suggest the high SO_2 observed during P2 resulted from long-range transport from Asia, which is likely from biomass burning emissions due to slash burn techniques in southeast Asian during this time of year.[50]

A number of sources exist for the amine precursors. The CV is largely inhabited by significant livestock populations which represent large sources of ammonia as well as amines.[51] Local sources of amines from vegetation[52] are likely negligible in comparison to bovine sources in the CV, which can be transported by the upslope/downslope system along with O_3. Overall, amines and O_3 likely came from agricultural emissions and photochemical pollution in the CV, respectively. During P1, lower SO_2 concentrations and correspondingly less sulfate (~4 times less in average sulfate peak area and number of particles containing sulfate as described in the Supporting Information) were observed compared to P2. In contrast, during P2 Asian-transported SO_2 likely from biomass burning emissions and more sulfate were observed, potentially leading to the faster average particle growth compared to P1.

NPF periods occurring after heavy precipitation periods began each day during low RH, high temperature, and peak solar radiation, and during pristine, nonprecipitating periods, demonstrating the strong dependence of NPF on ambient conditions. Growth of newly formed particles occurred as RH increased and temperature and solar radiation decreased, and was relatively fast compared to previous observations, which can be attributed to the extremely clean conditions as well as the availability of gas-phase SO_2, O_3, and amines. Using UF-ATOFMS, increases in the overall fraction of amine-containing particles from $100 \leq D_{va} \leq 1000$ nm occurred over the course of the NPF events after substantial particle growth from the smallest sizes. During NPF, amine and sulfate ion markers are observed in the same, single-particle mass spectra, and the number of particles containing sulfate correlated 1:1 to the number of amine-containing particles but not ammonium-containing particles. Although we cannot determine all of the sources of the species involved in these processes, air mass trajectories suggest the amines and O_3 came from animal husbandries and vehicle pollution in the CV, respectively, while SO_2 was likely transported from Asia during P2.

It is important to understand and characterize such small particles that ultimately can activate as CCN and impact cloud formation and potentially precipitation over the Sierra Nevada. One of the new and more intriguing findings of this work is the key role long-range transported SO_2 from Asia played in CCN formation in the Sierra Nevada. We hypothesize that SO_2 formed sulfate which reacted with amines to form aminium-sulfate salts, particularly during P2 when SO_2 concentrations and particles containing sulfate were highest, ultimately leading to CCN-active particles upon growth to larger sizes. To further quantify the ability of organic salts to activate as CCN, laboratory studies to measure the hygroscopicity parameter kappa (κ) of various aminium-sulfate salts will be performed.[53] The range of κ values at Sugar Pine (0.013−0.16) suggest the CCN-active particles contained organic species.[53] The presence of aminium salts, which are known to be water-soluble,[41,42] could account for the more hygroscopic and CCN-active particles measured during NPF events. A recently completed field study over Sugar Pine and the CV will allow comparisons between ground and measurements aloft to gain further insight into the regional impact of newly formed particles on orographic clouds and precipitation in this region.

■ ASSOCIATED CONTENT

Supporting Information. Details from SMPS data during NPF events, calculated GRs, mass spectra, descriptions of the particles types, mass spectra peak areas, additional FLEXPART analysis, OMI images, and miscellaneous discussion. This material is available free of charge via the Internet at http://pubs.acs.org.

■ AUTHOR INFORMATION

Corresponding Author

*Phone: 858-822-5312; fax: 858-534-7042; e-mail: kprather@ucsd.edu.

Present Addresses

⊥Department of Chemistry, University of Iowa, Iowa City, IA, 52242

■ ACKNOWLEDGMENT

The Forest Hill Power Utility District is acknowledged for hosting the sampling site. Joseph Mayer, Cassandra Gaston, Dr. Meagan Moore, and Melanie Zauscher are acknowledged for assisting in preparing instrumentation for the study and setting up the site. Also, Professor Joel Norris is acknowledged for assistance with species source determination.

■ REFERENCES

(1) Solomon, S.; Qin, D.; Manning, M.; Chen, Z.; Marquis, M.; Averyt, K. B.; Tignor, M. "Climate Change 2007: The Physical Science Basis, Contribution of Working Group I to the Fourth Assessment Report of the Intergovernmental Panel on Climate Change," Cambridge Univ. Press: New York, 2007.

(2) Albrecht, B. A. Aerosols, cloud microphysics, and fractional cloudiness. *Science* **1989**, *245*, 1227–1230.

(3) Twomey, S. Influence of pollution on shortwave albedo of clouds. *J. Atmos. Sci.* **1977**, *34*, 1149–1152.

(4) Ziemba, L. D.; Dibb, J. E.; Griffin, R. J.; Huey, L. G.; Beckman, P. Observations of particle growth at a remote, Arctic site. *Atmos. Environ.* **2010**, *44*, 1649–1657.

(5) Ristovski, Z. D.; Suni, T.; Kulmala, M.; Boy, M.; Meyer, N. K.; Duplissy, J.; Turnipseed, A.; Morawska, L.; Baltensperger, U. The role of sulphates and organic vapours in growth of newly formed particles in a eucalyptus forest. *Atmos. Chem. Phys.* **2010**, *10*, 2919–2926.

(6) Seinfeld, J. H.; Pandis, S. N. *Atmospheric Chemistry and Physics*, 2nd ed.; John Wiley & Sons, Inc.: New York, 2006.

(7) Kulmala, M.; Pirjola, U.; Makela, J. M. Stable sulphate clusters as a source of new atmospheric particles. *Nature* **2000**, *404*, 66–69.

(8) Ortega, I. K.; Kurten, T.; Vehkamaki, H.; Kulmala, M. The role of ammonia in sulfuric acid ion induced nucleation. *Atmos. Chem. Phys.* **2008**, *8*, 2859–2867.

(9) Lunden, M. M.; Black, D. R.; Mckay, M.; Revzan, K. L.; Goldstein, A. H.; Brown, N. J. Characteristics of fine particle growth events observed above a forested ecosystem in the Sierra Nevada Mountains of California. *Aerosol Sci. Technol.* **2006**, *40*, 373–388.

(10) Fisher, J. A.; Jacob, D. J.; Purdy, M. T.; Kopacz, M.; Le Sager, P.; Carouge, C.; Holmes, C. D.; Yantosca, R. M.; Batchelor, R. L.; Strong, K.; Diskin, G. S.; Fuelberg, H. E.; Holloway, J. S.; Hyer, E. J.; McMillan, W. W.; Warner, J.; Streets, D. G.; Zhang, Q.; Wang, Y.; Wu, S. Source attribution and interannual variability of Arctic pollution in spring constrained by aircraft (ARCTAS, ARCPAC) and satellite (AIRS) observations of carbon monoxide. *Atmos Chem Phys* **2010**, *10*, 977–996.

(11) Wang, L.; Khalizov, A. F.; Zheng, J.; Xu, W.; Ma, Y.; Lal, V.; Zhang, R. Atmospheric nanoparticles formed from heterogeneous reactions of organics. *Nat. Geosci.* **2010**, *3*, 238–242.

(12) Kulmala, M.; Kerminen, V. M.; Laaksonen, A. Simulations on the effect of sulphuric acid formation on atmospheric aerosol concentrations. *Atmos. Environ.* **1995**, *29*, 377–382.

(13) Wehner, B.; Petaja, T.; Boy, M.; Engler, C.; Birmili, W.; Tuch, T.; Wiedensohler, A.; Kulmala, M. The contribution of sulfuric acid and non-volatile compounds on the growth of freshly formed atmospheric aerosols. *Geophys. Res. Lett.* **2005**, *32*, L17810, doi:17810.11029/12005GL023827.

(14) Smith, J. N.; Barsanti, K. C.; Friedli, H. R.; Ehn, M.; Kulmala, M.; Collins, D. R.; Scheckman, J. H.; Williams, B. J.; McMurry, P. H. Observations of aminium salts in atmospheric nanoparticles and possible climatic implications. *Proc. Natl. Acad. Sci. U.S.A.* **2009**, *107*, 6634–6639.

(15) McMurry, P. H.; Fink, M.; Sakurai, H.; Stolzenburg, M. R.; Mauldin, R. L.; Smith, J.; Eisele, F.; Moore, K.; Sjostedt, S.; Tanner, D.; Huey, L. G.; Nowak, J. B.; Edgerton, E.; Voisin, D. A criterion for new particle formation in the sulfur-rich Atlanta atmosphere. *J. Geophys. Res.* **2005**, *110*, D22S02, doi:10.1029/2005JD005901.

(16) Barsanti, K. C.; McMurry, P. H.; Smith, J. N. The potential contribution of organic salts to new particle growth. *Atmos. Chem. Phys. Discuss.* **2009**, *9*, 2949–2957.

(17) Mäkelä, J. M.; Yli-Koivisto, S.; Hiltunen, V.; Seidl, W.; Swietlicki, E.; Teinila, K.; Sillanpaa, M.; Koponen, I. K.; Paatero, J.; Rosman, K.; Hameri, K. Chemical composition of aerosol during particle formation events in boreal forest. *Tellus B* **2001**, *53*, 380–393.

(18) Wang, L.; Lal, V.; Khalizov, A. F.; Zhang, R. Heterogeneous chemistry of alkylamines with sulfuric acid: Implications for atmospheric formation of alkylaminium sulfates. *Environ. Sci. Technol.* **2010**, *44*, 2461–2465.

(19) Murphy, S. M.; Sorooshian, A.; Kroll, J. H.; Ng, N. L.; Chhabra, P.; Tong, C.; Surratt, J. D.; Knipping, E.; Flagan, R. C.; Seinfeld, J. H. Secondary aerosol formation from atmospheric reactions of aliphatic amines. *Atmos. Chem. Phys.* **2007**, *7*, 2313–2337.

(20) Smith, J. N.; Moore, K. F.; McMurry, P. H.; Eisele, F. L. Atmospheric measurements of sub-20 nm diameter particle chemical composition by thermal desorption chemical ionization mass spectrometry. *Aerosol. Sci. Tech.* **2004**, *38*, 100–110.

(21) Rosenfeld, D.; Woodley, W. L.; Axisa, D.; Freud, E.; Hudson, J. G.; Givati, A. Aircraft measurements of the impacts of pollution aerosols on clouds and precipitation over the Sierra Nevada. *J. Geophys. Res.* **2008**, *113*, D15203, doi:15210.11029/12007JD00954.

(22) Roberts, G. C.; Nenes, A. A continuous-flow streamwise thermal-gradient CCN chamber for atmospheric measurements. *Aerosol Sci. Technol.* **2005**, *39*, 206–221.

(23) Gard, E.; Mayer, J. E.; Morrical, B. D.; Dienes, T.; Fergenson, D. P.; Prather, K. A. Real-time analysis of individual atmospheric aerosol particles: Design and performance of a portable ATOFMS. *Anal. Chem.* **1997**, *69*, 4083–4091.

(24) Su, Y. X.; Sipin, M. F.; Furutani, H.; Prather, K. A. Development and characterization of an aerosol time-of-flight mass spectrometer with increased detection efficiency. *Anal. Chem.* **2004**, *76*, 712–719.

(25) Spencer, M. T.; Prather, K. A. Using ATOFMS to determine OC/EC mass fractions in particles. *Aerosol Sci. Technol.* **2006**, *40*, 585–594.

(26) Song, X. H.; Hopke, P. K.; Fergenson, D. P.; Prather, K. A. Classification of single particles analyzed by ATOFMS using an artificial neural network, ART-2A. *Anal. Chem.* **1999**, *71*, 860–865.

(27) Covert, D. S.; Kapustin, V. N.; Quinn, P. K.; Bates, T. S. New particle formation in the marine boundary-layer. *J. Geophys. Res.* **1992**, *97*, 20581–20589.

(28) Hansen, A. D. A.; Rosen, H. Horizontal inhomogeneities in the particulate carbon component of the Arctic haze. *Atmos. Environ.* **1985**, *19*, 2175–2180.

(29) Hitzenberger, R.; Tohno, S. Comparison of black carbon (BC) aerosols in two urban areas - concentrations and size distributions. *Atmos. Environ.* **2001**, *35*, 2153–2167.

(30) Berndt, T.; Stratmann, F.; Sipila, M.; Vanhanen, J.; Petaja, T.; Mikkila, J.; Gruner, A.; Spindler, G.; Mauldin, R. L., III; Curtius, J.; Kulmala, M.; Heintzenberg, J. Laboratory study on new particle formation from reaction OH + SO_2: influence of experimental conditions, H_2O vapour, NH_3 and the amine *tert*-butylamine on the overall process. *Atmos. Chem. Phys.* **2010**, *10*, 6447–6484.

(31) Kulmala, M.; Vehkamaki, H.; Petaja, T.; Dal Maso, M.; Lauri, A.; Kerminen, V. M.; Birmili, W.; McMurry, P. H. Formation and growth rates of ultrafine atmospheric particles: a review of observations. *J. Aerosol Sci.* **2004**, *35*, 143–176.

(32) Sharkey, T. D.; Loreto, F. Water-stress, temperature, and light effects on the capacity for isoprene emission and photosynthesis of Kudzu leaves. *Oecologia* **1993**, *95*, 328–333.

(33) Merikanto, J.; Spracklen, D. V.; Mann, G. W.; Pickering, S. J.; Carslaw, K. S. Impact of nucleation on global CCN. *Atmos. Chem. Phys. Discuss* **2009**, *9*, 12999–13037.

(34) Kerminen, V. M.; Lihavainen, H.; Komppula, M.; Viisanen, Y.; Kulmala, M. Direct observational evidence linking atmospheric aerosol formation and cloud droplet activation. *Geophys. Res. Lett.* **2005**, *32*, L14803, doi:14810.11029/12005GL02313.

(35) Kuang, C.; McMurry, P. H.; McCormick, A. V. Determination of cloud condensation nuclei production from measured new particle formation events. *Geophys. Res. Lett.* **2009**, *36*, L09822, doi:09810.01029/02009GL037584.

(36) Pierce, J. R.; Adams, P. J. Efficiency of cloud condensation nuclei formation from ultrafine particles. *Atmos. Chem. Phys.* **2007**, *7*, 1367–1379.

(37) Sihto, S.-L.; Mikkila, J.; Vanhansen, J.; Ehn, M.; Liao, L.; Lehtipalo, K.; Aalto, P. P.; Duplissy, J.; Petaja, T.; Kerminen, V. M.; Boy, M.; Kulmala, M. Seasonal variation of CCN concentrations and aerosol activation properties in boreal forest. *Atmos. Chem. Phys. Discuss.* **2010**, *10*, 28231–28272.

(38) O'Halloran, T. L.; Fuentes, J. D.; Collins, D. R.; Cleveland, M. J.; Keene, W. C. Influence of air mass source region on nanoparticle events and hygroscopicity in central Virginia, US. *Atmos. Environ.* **2009**, *43*, 3586–3595.

(39) Friedman, B.; Herich, H.; Kammermann, L.; Gross, D. S.; Arneth, A.; Holst, T.; Cziczo, D. J. Subarctic atmospheric aerosol composition: 1. Ambient aerosol characterization. *J. Geophys. Res.* **2009**, *114*, D13203, doi:13210.11029/12009JD011772.

(40) Chang, L. S.; Schwartz, S. E.; McGraw, R.; Lewis, E. R. Sensitivity of aerosol properties to new particle formation mechanism

and to primary emissions in a continental-scale chemical transport model. *J. Geophys. Res.* **2009**, *114*, D07203, doi:07210.01029/02008JD011019.

(41) Angelino, S.; Suess, D. T.; Prather, K. A. Formation of aerosol particles from reactions of secondary and tertiary alkylamines: Characterization by aerosol time-of-flight mass spectrometry. *Environ. Sci. Technol.* **2001**, *35*, 3130–3138.

(42) Pratt, K. A.; Hatch, L. E.; Prather, K. A. Seasonal volatility dependence of ambient particle phase amines. *Environ. Sci. Technol.* **2009**, *43*, 5276–5281.

(43) Finlayson-Pitts, B. J.; Pitts, J. N. *Chemistry of the Upper and Lower Atmosphere*; Academic Press: San Diego, 2000.

(44) Bzdek, B. R.; Ridge, D. P.; Johnston, M. V. Size-dependent reactions of ammonium bisulphate clusters with dimethylamine. *J. Phys. Chem. A* **2010**, *114*, 11638–11644.

(45) Stohl, A.; Hittenberger, M.; Wotawa, G. Validation of the Lagrangian particle dispersion model FLEXPART against large-scale tracer experiment data. *Atmos. Environ.* **1998**, *32*, 4245–4264.

(46) Stohl, A.; Forster, C.; Frank, A.; Seibert, P.; Wotawa, G. Technical note: The Lagrangian particle dispersion model FLEXPART version 6.2. *Atmos. Chem. Phys.* **2005**, *5*, 2461–2474.

(47) Collett, J. L.; Daube, B. C.; Gunz, D.; Hoffmann, M. R. Intensive studies of Sierra-Nevada cloudwater chemistry and its relationship to precursor aerosol and gas concentrations. *Atmos. Environ. A-Gen.* **1990**, *24*, 1741–1757.

(48) Bao, J. W.; Michelson, S. A.; Persson, P. O. G.; Djalalova, I. V.; Wilczak, J. M. Observed and WRF-simulated low-level winds in a high-ozone episode during the Central California Ozone Study. *J. Appl. Meteorol. Clim.* **2008**, *47*, 2372–2394.

(49) Nilsson, E. D.; Rannik, U.; Kulmala, M.; Buzorius, G.; O'Dowd, C. D. Effects of continental boundary layer evolution, convection, turbulence and entrainment, on aerosol formation. *Tellus B* **2001**, *53*, 441–461.

(50) Streets, D. G.; Yarber, K. F.; Woo, J. H.; Carmichael, G. R. Biomass burning in Asia: Annual and seasonal estimates and atmospheric emissions. *Global Biogeochem. Cycles* **2003**, *17*.

(51) Sorooshian, A.; Murphy, S. N.; Hersey, S.; Gates, H.; Padro, L. T.; Nenes, A.; Brechtel, F. J.; Jonsson, H.; Flagan, R. C.; Seinfeld, J. H. Comprehensive airborne characterization of aerosol from a major bovine source. *Atmos. Chem. Phys.* **2008**, *8*, 5489–5520.

(52) Neff, J. C.; Holland, E. A.; Dentener, F. J.; McDowell, W. H.; Russell, K. M. The origin, composition and rates of organic nitrogen deposition: A missing piece of the nitrogen cycle? *Biogeochemistry* **2002**, *57*, 99–136

(53) Petters, M. D.; Kreidenweis, S. M. A single parameter representation of hygroscopic growth and cloud condensation nucleus activity. *Atmos. Chem. Phys.* **2007**, *7*, 1961–1971.